JBC RESEARCH ARTICLE

An *in vitro* reconstitution system to monitor iron transfer to the active site during the maturation of [NiFe]-hydrogenase

Received for publication, June 6, 2022, and in revised form, July 13, 2022 Published, Papers in Press, July 20, 2022,
https://doi.org/10.1016/j.jbc.2022.102291

Basem Soboh[1,*], **Lorenz Adrian**[2,3], **and Sven T. Stripp**[4]

From the [1]*Department of Physics, Genetic Biophysics, Freie Universität Berlin, Berlin, Germany;* [2]*Department of Environmental Biotechnology, Helmholtz Centre for Environmental Research–UFZ, Leipzig, Germany;* [3]*Chair of Geobiotechnology, Technische Universität Berlin, Berlin, Germany; and* [4]*Department of Physics, Experimental Molecular Biophysics, Freie Universität Berlin, Berlin, Germany*

Edited by Ruma Banerjee

[NiFe]-hydrogenases (Hyds) comprise a small and a large subunit. The latter harbors the biologically unique [NiFe](CN)$_2$CO active-site cofactor. The maturation process includes the assembly of the [Fe](CN)$_2$CO cofactor precursor, nickel binding, endoproteolytic cleavage of the large subunit, and dimerization with the small subunit to yield active enzyme. The biosynthesis of the [Fe](CN)$_2$CO moiety of [NiFe]-Hyd-1 and Hyd-2 occurs on the scaffold complex HybG–HypD (GD), whereas the HypC–HypD complex is specific for the assembly of Hyd-3. The metabolic source and the route for delivering iron to the active site remain unclear. To investigate the maturation process of O$_2$-tolerant Hyd-1 from *Escherichia coli*, we developed an enzymatic *in vitro* reconstitution system that allows for the synthesis of Hyd-1 using only purified components. Together with this *in vitro* reconstitution system, we employed biochemical analyses, infrared spectroscopy (attenuated total reflection FTIR), mass spectrometry (MS), and microscale thermophoresis to monitor the iron transfer during the maturation process and to understand how the [Fe](CN)$_2$CO cofactor precursor is ultimately incorporated into the large subunit. We demonstrate the direct transfer of iron from ^{57}Fe-labeled GD complex to the large subunit of Hyd-1. Our data reveal that the GD complex exclusively interacts with the large subunit of Hyd-1 and Hyd-2 but not with the large subunit of Hyd-3. Furthermore, we show that the presence of iron in the active site is a prerequisite for nickel insertion. Taken together, these findings reveal how the [Fe](CN)$_2$CO cofactor precursor is transferred and incorporated into the active site of [NiFe]-Hyd.

Hydrogenases (Hyds) are microbial metalloenzymes that catalyze the reduction of protons to H_2 (disposal of excess reducing equivalents) or the oxidation of H_2 as an energy source (1–3). Based on the metal content at the active site, [FeFe]–, [NiFe]–, and iron sulfur cluster-free Hyds are distinguished (2, 3). While [FeFe]-Hyds are typically monomeric, [NiFe]-Hyds are formed by a heterodimer of a large and a small subunit. The large subunit harbors the [NiFe]-cofactor, whereas the small subunit contains 1 to 3 iron sulfur clusters involved in electron transfer (4). The [NiFe]-Hyd heterodimer can be associated with additional subunits, for example, for transferring electrons to pyridine nucleotides or for anchoring multimeric enzymes to the membrane (2).

Escherichia coli synthesizes 3 membrane-bound [NiFe]-Hyds. Although they carry the same [NiFe]-cofactor, Hyd-1 and Hyd-2 are H_2-oxidizing enzymes, whereas Hyd-3 is a H_2-evolving enzyme. Each of the 3 Hyds is predicted to contribute to different aspects of cellular metabolism (5, 6). The O_2-tolerant Hyd-1 is able to oxidize H_2 in the presence of oxygen (air) and has become one of the most important paradigm systems for understanding O_2-tolerant Hyds (7). The O_2-sensitive Hyd-2 couples H_2 oxidation to quinone reduction during anaerobic respiration (5, 8, 9). Hyd-3 forms a complex with the H_2-evolving formate hydrogenlyase, which acts to detoxify excess formic acid into CO_2 and H_2 during fermentation (10).

The [NiFe]-Hyds of *E. coli* are activated by a specific maturation apparatus. Figure 1 shows the current understanding of the maturation of Hyd-1 and Hyd-2. The complex machinery involved in the synthesis of the [NiFe]-cofactor and its insertion into the apo-form of the large subunit comprises several maturation proteins (11, 12). The assembly of the [Fe](CN)$_2$CO moiety (steps 1–3 in Fig. 1) suggests the following sequence of events: (1) the HybG dimer is proposed to deliver both iron and CO_2 to HypD (13). Subsequently, the HybG–HypD (GD) complex is formed while a HybG monomer is released (14). (2) The GD complex is proposed to catalyze an ATP-dependent reduction of CO_2 (15); however, definite proof for this enzymatic activity is yet to obtain. (3) The synthesis of the CN^- ligands from carbamoyl phosphate in an ATP-dependent condensation reaction is catalyzed by HypF and HypE (16). Subsequently, cyanide is transferred to the iron ion, which induces the formation of the [Fe](CN)$_2$CO moiety on the GD complex (17–19). It is unknown how the cofactor precursor is transferred to the large subunit, but once the assembly and insertion of the cofactor are completed (step 4 and 5 in Fig. 1), the C terminus of the large subunit is cleaved off (step 6). This results in conformational changes that allow dimerization with the small subunit, which yields the active enzyme (step 7) (20, 21).

* For correspondence: Basem Soboh, basem.soboh@fu-berlin.de.

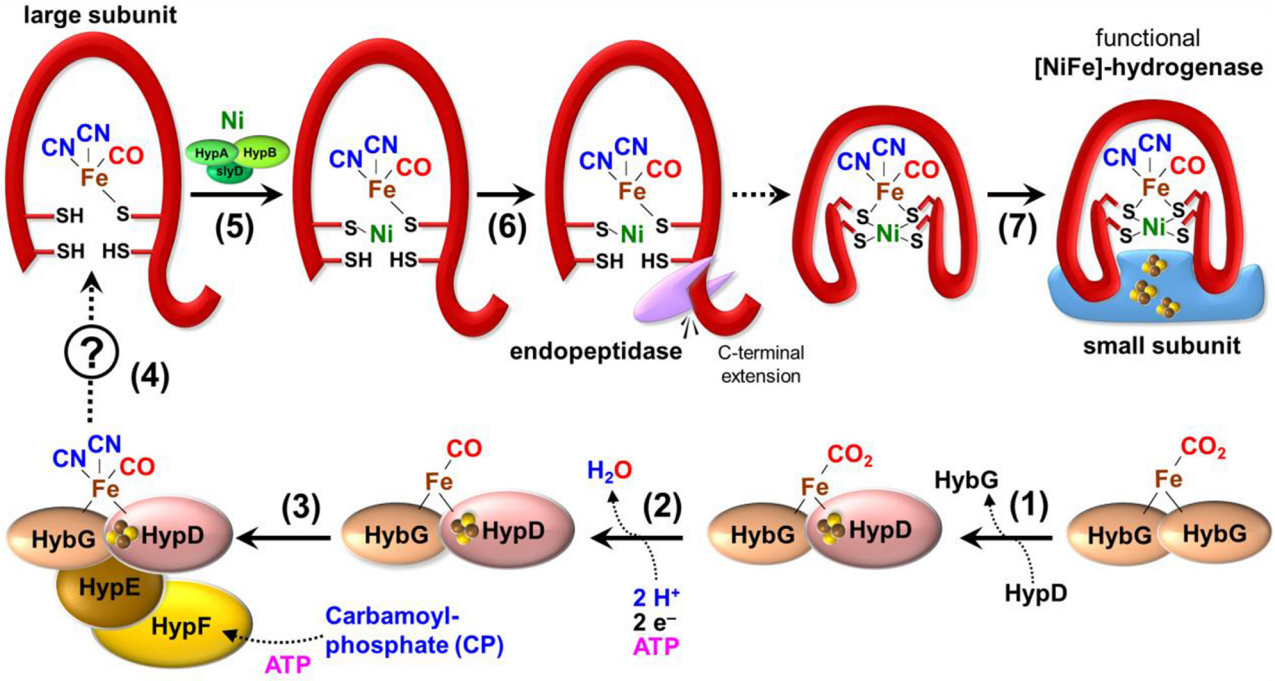

Figure 1. Working model for maturation of the large subunit of Hyd-1 and Hyd-2 of *Escherichia coli* into functional [NiFe]-Hyd. (1) The HybG–HypD complex is formed upon contact with the [Fe]CO_2 carrying HybG dimer. (2) The CO_2 ligand may undergo an ATP-dependent reduction to CO catalyzed by HybG–HypD complex. (3) The maturation proteins HypF and HypE catalyze the synthesis and transfer of CN^- ligands to the CO-modified iron ion and formation of the [Fe]$(CN)_2CO$ moiety on the HybG–HypD complex. (4) It is unclear how the [Fe]$(CN)_2CO$ moiety is incorporated into the large subunit. (5) Nickel insertion by concerted activity of HypA, HypB, and SlyD. (6) Endoproteolytic cleavage of the C-terminal peptide, associated with conformational changes of the protein. (7) Dimerization of large and small subunits form functional [NiFe]-Hyd. Hyd, hydrogenase.

The GD complex is the heart of the maturation machinery of Hyd-1 and Hyd-2 (22, 23). It is the synthesis platform, where the CN^- and CO ligands are attached to the iron ion of the cofactor. The transfer of each CN^- ligand to the iron ion on the GD complex requires the input of 2 electrons (17, 24). In addition, 2 electrons are required for CO_2 reduction if CO_2 is the metabolic precursor of CO (14). HypD must be involved in electron transfer because it is the only maturation enzyme that carries an [4Fe–4S] cluster. In a recent study, we proposed a unique redox cascade between the [4Fe–4S] cluster and a conserved disulfide motif of HypD. This provided comprehensive evidence for an electron inventory fit to drive multi–electron redox reactions required for the attachment of the CN^- and CO ligands to the iron ion (14).

Although all 3 Hyds carry the same [NiFe]$(CN)_2CO$ cofactor, orthologous accessory proteins for the maturation of each Hyd have been described (11). For example, The C-terminal extension of the large subunit of each enzyme is cleaved off by a specific endopeptidase (25). Furthermore, the HybG homolog HypC forms the HypC–HypD (CD) complex with HypD that exclusively catalyzes the assembly of the [Fe]$(CN)_2CO$ moiety of Hyd-3 (23). Table 1 describes the function of proteins and enzymes involved in the maturation of [NiFe]-Hyd that used in this study.

Table 1
The proposed function of [NiFe]-Hyd proteins used in this study

Protein	Molecular weight (kDa)	Function/properties	References
HyaB	66.5	Large subunit of Hyd-1	(10)
HyaA	41	Small subunit of Hyd-1	(49)
HybC	63.5	Large subunit of Hyd-2	(10)
HycE	65	Large subunit of Hyd-3	(49)
HybG	8.7	Forms the GD complex with HypD, involved in assembly of the [Fe]$(CN)_2CO$ moiety of Hyd-1 and Hyd-2	(22, 23)
HypC	10	Forms the CD complex with HypD, involved in assembly of the [Fe]$(CN)_2CO$ moiety of Hyd-3	(17, 50)
HypD	41.4	Iron sulfur scaffold protein, involved in assembly of the [Fe]$(CN)_2CO$ of the 3 Hyds, shows ATPase activity, and catalyzes CO-dependent reduction of MV	(15, 37)
HypE	35	ATPase, HypE forms the HypEF complex with HypF, involved in synthesis and transfer of the CN^- ligands	(18, 51)
HypF	82	Carbamoyl phosphate phosphatase, carbamoyl-transferase, ATPase, involved in CN^- synthesis	(16)
HyaD	22	C-terminal cleavage of the Hyd-1 large subunit	(26)

Much is known about the maturation of [NiFe]-Hyd, but the metabolic source(s) and the iron transfer to the active site remains an open question. In the present work, we introduce a novel *in vitro* reconstitution system for the biosynthesis of Hyd-1 from *E. coli* and employ it together with biochemical analyses, infrared spectroscopy, MS, and protein interaction studies, to monitor the iron transfer during the maturation process, which allows understanding how the $[Fe](CN)_2CO$ cofactor precursor is specifically incorporated into the large subunit of Hyd-1.

Results

An in vitro *reconstitution system to study the maturation of Hyd-1*

In this study, an enzymatic *in vitro* maturation assay has been established that allows synthesizing functional [NiFe]-Hyd Hyd-1 of *E. coli*. This reconstitution system contains only purified components, that is, the apo-form of the large subunit of Hyd-1 (referred to as pre-HyaB), the GD complex, the accessory proteins HypE and HypF, and an activation mix (AM). The reaction was started by addition of the Hyd-1-specific endopeptidase HyaD, which cleaves the C terminus of HyaB by 15 amino acids (22, 26). After incubation for 15 and 30 min, aliquots of the reaction mixture were analyzed by SDS-PAGE for cleavage of pre-HyaB into processed HyaB (Fig. 2, lanes 4 and 5). No cleavage of pre-HyaB could be observed when the reaction was performed in the absence of endopeptidase HyaD (lane 1), under aerobic conditions (lane 2), or in the absence of AM (lane 3). Since HyaB is the only Strep-tagged protein, it can be easily isolated from the reaction mix by Strep-Tactin affinity chromatography. Lane 6 shows both unprocessed pre-HyaB and processed HyaB isolated from the reaction assay after 30 min, whereas a completely processed form of HyaB was isolated from the reaction mix only after 60 min incubation (lane 9). A ^{His}HyaA-enriched fraction (lane 7) was mixed with a fraction of ^{Strep}HyaB that was isolated from the reaction mixture after 30 min to reconstitute the active Hyd-1 heterodimer (lane 8). Quality control by attenuated total reflection (ATR) FTIR spectroscopy showed the CO/CN^- vibrational fingerprint of the cofactor of the *in vitro* matured Hyd-1 enzyme (Fig. S1). In the absence of the GD complex, HypE, HypF, or AM, the absorption bands of CN^- and CO were not observed.

Analysis of Hyd-1 activity reconstituted in vitro

Like all [NiFe]-Hyds, the catalytic large subunit of Hyd-1 (HyaB) alone does not exhibit Hyd activity (20, 21). Therefore, the purified small subunit of Hyd-1 (HyaA) was added to *in vitro* reconstituted HyaB yielding the active Hyd-1 heterodimer. Various preparations of *in vitro* reconstituted Hyd-1 were analyzed for H_2 oxidation activity by following H_2-dependent reduction of benzyl viologen (BV) photometrically (Fig. 3*A*). The maximal activity was obtained when all components of the *in vitro* assay were present ("complete"). The specific activity was 0.75 ± 0.17 μmol H_2 oxidized per min^{-1} mg^{-1}. This value is close to the specific activity of Hyd-1

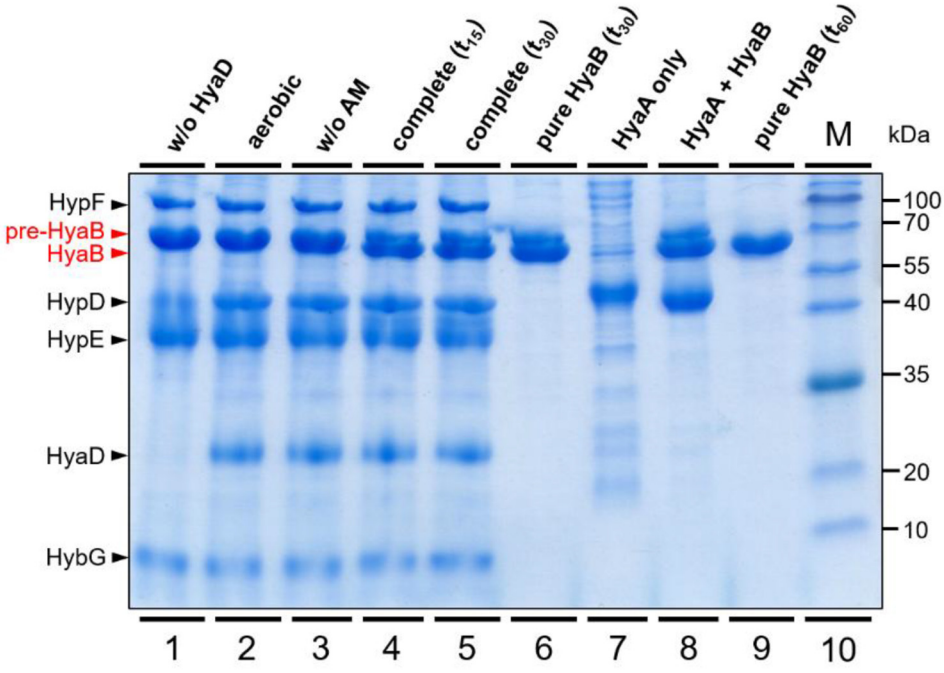

Figure 2. *In vitro* reconstitution system of Hyd-1 of *Escherichia coli*. SDS-PAGE analysis of the *in vitro* assay at different maturation steps. The complete assay includes purified ^{Strep}HyaB, ^{His}GD complex, ^{His}HypE and ^{His}HypF, the endopeptidase ^{His}HyaD, and the activation mix (AM). No cleavage of HyaB was observed in the absence of endopeptidase HyaD (lane 1, w/o HyaD) or under aerobic conditions (lane 2, aerobic) or without AM (lane 3, w/o AM). Lanes 4 and 5: aliquots of the reaction mix were analyzed after 15 and 30 min incubation (t_{15}, t_{30}), respectively. Lane 6: unprocessed and processed HyaB isolated from the reaction assay after 30 min incubation. Lane 7: The Hyd-1 small subunit ^{His}HyaA only. Lane 8: The HyaB fraction (t_{30}) was mixed with ^{His}HyaA, and the mixture was applied to Strep-Tactin chromatography. Lane 9: Completely processed ^{Strep}HyaB was isolated from the reaction mix after 60 min incubation time. Lane 10: 5 μl of marker proteins of known size (page ruler protein ladder). GD, HybG–HypD; Hyd, hydrogenase.

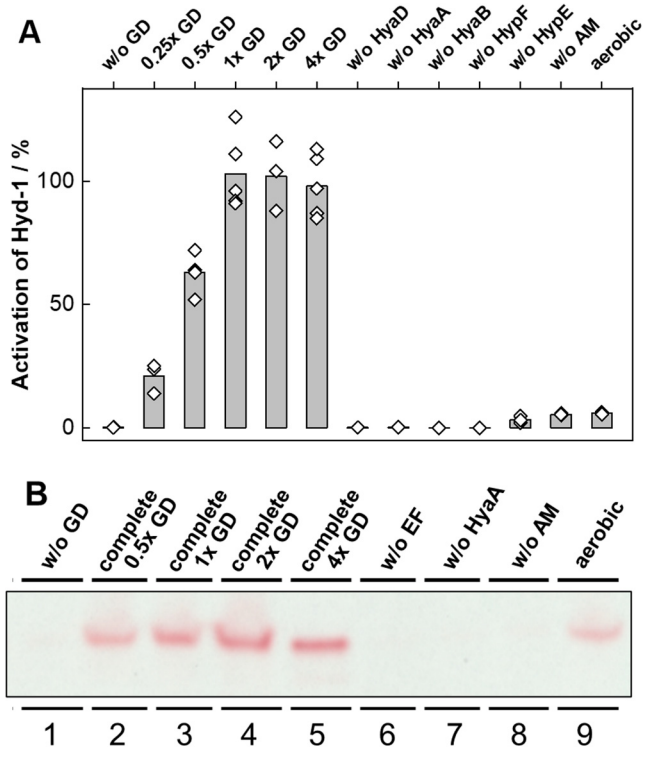

Figure 3. Kinetic analysis of H_2-uptake activity of the *in vitro* matured Hyd-1. *A*, the complete assay was composed of purified HyaB, GD complex, HypE, HypF, the endopeptidase HyaD, HyaA, and activation mix (AM). Reactions were conducted in the absence of 1 or more substrates at a time as indicated. The samples were analyzed for activity by following H_2-dependent reduction of benzyl viologen photometrically. The maximal attainable activation (100%) was in the presence of all components of the *in vitro* assay (complete). *B*, analysis of various reactions of the *in vitro* matured Hyd-1 using in-gel activity staining. Aliquots of reaction mix (15 µl) were mixed with the small subunit HyaA, separated by native-PAGE and followed by activity stain specific for H_2-oxidizing Hyds. Lanes 2 to 5: The Hyd-1 activity band was observed when reaction mixture was complete. No Hyd-1 band was detected in the absence of GD complex (lane 1), without HypEF (lane 6), without HyaA (lane 7), or without AM (lane 8). Note lower intensity of the activity band when Hyd-1 was reconstituted under aerobic conditions (lane 9). GD, HybG–HypD; Hyd, hydrogenase.

as isolated from *E. coli* (27) and represents the maximum activity of 100%. Our data indicate that the Hyd-1 activity is proportional to the amount of the GD complex added to the *in vitro* assay, whereas adding higher molar ratios of the GD complex did not increase the Hyd-1 activity. It appears that the optimal amount of GD complex is at a 1:1 stoichiometry (columns 1–6 in Fig. 3*A*). To define the minimal combination of components that is sufficient to achieve complete maturation, several reactions were conducted in the absence of 1 or more substrates (Fig. 3*A*). Only background activity was observed when the GD complex, HyaD, HyaA, HyaB, HypF, HypE, or AM were omitted from the assay. Furthermore, only residual activity was measured when the maturation assay was performed under aerobic conditions. Together, these findings indicate that all proteins involved in the maturation assay are necessary and participate directly in the maturation process. Moreover, the *in vitro* system established in this study was applied to confirm the activity of individual proteins involved in the assay. From a previous study on Hyd-2 of *E. coli* (20, 22), increasing amounts of individual components were titrated into reaction assays, and the enzyme activity was only restored when maturation assays were complemented with the missing protein. In this study, a titration of Hyd-1 against the GD complex with all other components (HypE, HypF, and HyaD) in excess was performed. The highest activities of Hyd-1 were obtained when the GD complex was added in equivalent stoichiometric amounts (1:1, Fig. 3). In addition, we observed similar trends by analyzing the activity of Hyd-1 using in-gel activity staining (Fig. 3*B*). HyaA was added to various compositions of the reaction mix and incubated for 30 min. Then, the mixes were separated by native PAGE, and the H_2 oxidation activity was followed by activity staining. The Hyd-1 activity band was only detected in lanes to which all components of the maturation reaction mixture were applied (lanes 2–5). Without HypEF, HyaA, or the AM, no Hyd-1 activity was detected (lanes 6–8). Moreover, the intensity of the activity band significantly decreased when Hyd-1 was reconstituted under aerobic conditions (lane 9). No activity band was observed when HyaB was omitted from reaction mix.

In the next step, we performed *in situ* ATR FTIR difference spectroscopy (28) to confirm the integrity of the $[NiFe](CN)_2CO$ active site of reconstituted Hyd-1 enzyme. Figure 4*A* shows a difference spectrum upon exchange the headspace above the Hyd-1 protein film from N_2 to 10% H_2. The data clearly comprise CN^- band features (2100–2050 cm^{-1}) and CO band features (1950–1850 cm^{-1}), indicative of an intact Ni–Fe cofactor. Here, negative bands are observed under N_2, whereas positive bands accumulate in the presence of H_2. The observed band positions are in excellent agreement with the previously assigned [NiFe]-cofactor states of Hyd-1 from *E. coli* (29–31) and demonstrate the enrichment of Ni-R2 and Ni-R3 (νCO 1922 and 1914 cm^{-1}, respectively) over Ni-L2 and Ni-L3 (νCO 1876 and 1866 cm^{-1}, respectively) under H_2. Smaller negative band features are assigned to cofactor states Ni-C and Ni-SI (νCO 1951 and 1930 cm^{-1}, respectively). These changes result from the oxidation of H_2 and the subsequent reduction of the [NiFe]-cofactor. When the enzyme was reduced by deuterium gas (D_2) instead, difference spectra show the time-dependent evolution of a broad band at 2500 cm^{-1} (Fig. S1). Similar traces have been assigned to HDO, which accumulates when D_2 is oxidized, and deuterium ions (D^+) recombine with OH^- ions from bulk H_2O (20). This band is a highly specific marker for H_2 oxidation activity and proves that Hyd-1 is catalytically active. To probe the inhibition of Hyd-1, we recorded difference spectra in the presence of O_2 and CO. Figure 4*B* demonstrates how the enzymes convert into the Ni-B state (νCO 1942 cm^{-1}) in the presence of 10% O_2, whereas Fig. 4*C* depicts the conversion into Ni-SCO (νCO 1928 cm^{-1}) under 10% CO (note the typical high-frequency Ni-CO band at 2061 cm^{-1}). Based on these data, an experimental band assignment is suggested that agrees well with the *in vivo* matured Hyd-1 from *E. coli* (Table 2).

Iron transfer from the GD complex to the large subunit

To monitor the iron transfer during the maturation process and to understand how the $[Fe](CN)_2CO$ moiety is ultimately

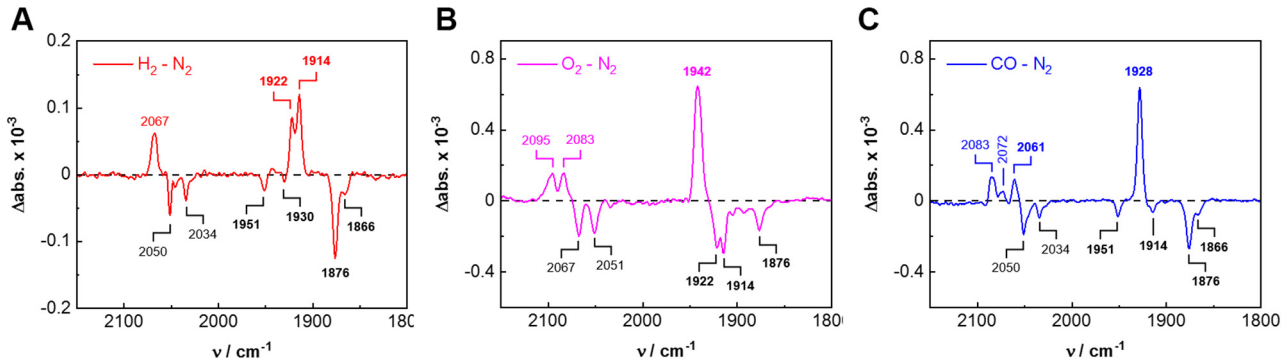

Figure 4. Infrared spectroscopy of *in vitro* matured Hyd-1. The CO and CN^- ligands are annotated in *bold* and *plain fonts*, respectively. *A*, the H_2–N_2 difference spectrum indicates the conversion of Ni-L2 into Ni-R2 and Ni-R3. Smaller negative bands are assigned to Ni-L3, Ni-C, and Ni-SI. *B*, in the presence of 10% O_2, Hyd-1 converges into the Ni-B state. Negative bands are assigned to Ni-R2 and Ni-R3, with a smaller contribution of Ni-L2. *C*, the CO-N_2 difference spectrum indicates the conversion of Ni-L2 into Ni-SCO (note the typical high-frequency Ni-CO band at 2061 cm^{-1}). Smaller negative bands are assigned to Ni-L3, Ni-C, and Ni-R3. The assignment is detailed in Table 2. Hyd, hydrogenase.

incorporated into the large subunit of Hyd-1, we employed our *in vitro* reconstitution system together with inductively coupled plasma (ICP)–MS, SDS-PAGE, and in-gel activity staining. Our strategy was as follows: (i) perform the *in vitro* assembly of Hyd-1 in the presence of purified ^{57}Fe-labeled GD complex. (ii) Isolate the catalytic subunit HyaB from the reaction mix. (iii) Analyze SDS-PAGE for cleavage of pre-HyaB into the processed form. (iv) Identification and quantification of ^{57}Fe and metal composition of trapped HyaB preparations by ICP–MS. (v) Supplementation of the *in vitro* reconstituted HyaB with the small subunit HyaA for activity analysis.

The results illustrated in Fig. 5, Fig. 6, and Table 3 reveal that *in vitro* processing of pre-HyaB and the subsequent activation of Hyd-1 correlate very well with the ^{57}Fe and nickel contents of HyaB. SDS-PAGE analysis indicates that only in the presence of all components in the *in vitro* maturation assay pre-HyaB was completely processed, and the maximal activation of Hyd-1 was achieved (lanes 2–4 in Fig. 5, reaction 1 and 2 in Table 3). Partial cleavage was observed by addition of 0.5 or 0.25 M ratio of the GD complex (lanes 5 and 6 in Fig. 5), and the activity was reduced by approximately 57% and 28%, respectively (reactions 3 and 4 in Table 3). Omission of nickel reduced the restored activity by approximately 22% suggesting that some nickel ions are delivered by the maturation proteins (lane 8 in Fig. 5, reaction 13 in Table 3). In addition, no cleavage and only residual activity were observed in control reactions containing the ^{57}Fe–GD complex that does not harbor the [Fe](CN)$_2$CO moiety. The ^{57}Fe–GD complex in these reactions was isolated either from a *ΔhypF*-mutant strain or had been treated with EDTA prior to incubation in the reconstitution reaction (lanes 9 and 10 in Fig. 5, reactions 5 and 6 in Table 3). Partial cleavage and a slightly reduced activation were observed when maturation assay was preformed aerobically (lane 11 in Fig. 5, reaction 9 in Table 3). Furthermore, partial cleavage of pre-HyaB was observed when the ^{57}Fe–GD complex was replaced by the ^{57}Fe–HypCD complex (lane 12 in Fig. 5); however, Hyd-1 activity could not be restored (reaction 8 in Table 3).

Metal analysis of the HyaB preparations isolated from various maturation assays indicates that the completely processed HyaB protein contains 1 mol ^{57}Fe and 1 mol nickel per mole protein (Table 3). The amount of copper and zinc was not significant. Up to a molar ratio of 1:1, the ^{57}Fe content of HyaB increases almost linearly with the amount of the GD complex in the reaction mix (Fig. 6 and reactions 1–4 in Table 3). The same trend is observed for nickel and the activation efficiency of Hyd-1. The ^{57}Fe molar ratio of HyaB isolated from maturation assays in which the GD complex was lacking the [Fe](CN)$_2$CO moiety was less than 0.2 ($GD^{\Delta hypF}$ in Fig. 6 and reactions 5, 6, and 11 in Table 3). For the first time, these data demonstrate that the source of ^{57}Fe on HyaB and Hyd-1 is the [Fe](CN)$_2$CO moiety of the GD complex.

When ^{57}Fe-HybG and ^{57}Fe-HypD were added to the reaction mix instead of the ^{57}Fe–GD complex, an ^{57}Fe molar ratio of 0.25 was detected, and the activity of Hyd-1 could not be restored (reaction 7). These results indicate that HybG and HypD individually cannot replace the GD complex and that the physical heterodimer of HybG and HypD is essential for a successful iron transfer. When the ^{57}Fe–GD complex was replaced by 3 equivalents of the ^{57}Fe–CD complex, an ^{57}Fe molar ratio of 0.38 was found; however, only background activity could be observed (reaction 8). When the reaction was performed under aerobic conditions, a ^{57}Fe molar ratio of 0.24 was detected, suggesting that iron transfer is inhibited by O_2 (reaction 9). In the absence of HypE and HypF, the ^{57}Fe content of HyaB was very low and Hyd-1 activity could not be

Table 2
Experimental band assignment and comparison with the literature (31)

State	*In vivo*	*In vitro*	Ni charge	Ligand
Ni-A	*n.o.*	*n.o.*	3+	OOH
Ni-B	1943	1942		OH
Ni-SI	1927	1930	2+	None
Ni-SCO	*n.o*	1928		CO
Ni-R1	*n.o.*	1948	2+	H
Ni-R2	1922	1922		
Ni-R3	1914	1914		
Ni-C	1949	1951	3+	H
Ni-L1	1898	1898	1+	None
Ni-L2	1877	1876		
Ni-L3	1867	1866		

Only the CO frequency is given.
n.o., not observed.

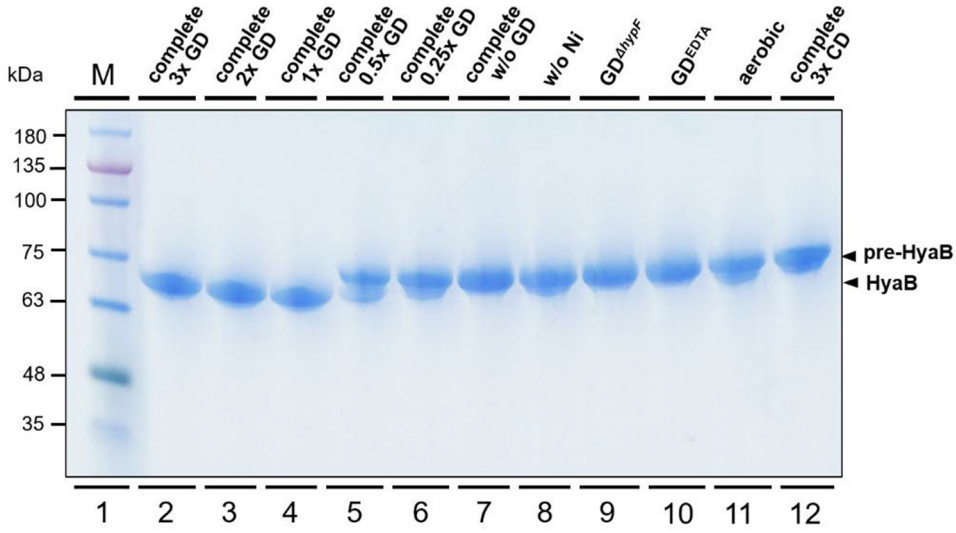

Figure 5. Analysis of HyaB processing. SDS-PAGE analysis for the *in vitro* processing of pre-HyaB. The complete assay includes purified HyaB, GD complex, HypE and HypF, HyaD, and AM. Complete cleavage of pre-HyaB only in the presence of all components of the *in vitro* system (lanes 2–4). Partial cleavage of pre-HyaB by adding limited amount of 0.5 or 0.25 M ratio of GD complex (lanes 5 and 6). No cleavage was observed without the GD complex or when GD was lacking the [Fe](CN)$_2$CO moiety (lanes 7, 9, and 10), and only partial cleavage can be observed in the absence of nickel (lane 8), or when reaction was performed aerobically (lane 11) or by replacing GD by CD complex (lane 12). AM, activation mix; CD, HypC-HypD; GD, HybG–HypD.

restored (reaction 14). HyaB matured in the absence of HyaD protease was found to contain a reduced ^{57}Fe molar ratio of 0.54 and a very low nickel content (reaction 15) suggesting a possible role of HyaD in the insertion of metal ions into HyaB. To determine whether the C-terminal extension of HyaB is required for the iron transfer, pre-HyaB was replaced by HyaB^{-15AA}. This genetic construct resembles pre-HyaB truncated for 15 amino acids at the C terminus. The HyaB^{-15AA} preparation could not restore Hyd-1 activity and was devoid of ^{57}Fe (Fig. 6 and reaction 10). These results are in line with our previous findings that the GD complex was not able to recognize HybC^{-15AA}, the large subunit of Hyd-2 from *E. coli* (20). Excluding nickel or the AM from the maturation assay reduced the activation efficiency of Hyd-1 to 22%; however, the ^{57}Fe content of HyaB was barely affected (Fig. 6 and reactions 12 and 13). In contrast, the presence of iron in the active site appears to be a prerequisite for nickel insertion. Our novel finding shown in Fig. 6 and reactions 1 to 14 that nickel insertion takes place only when iron has been inserted before. Together, these data show that iron was exclusively incorporated into HyaB under conditions where a full assembly of the [NiFe]-cofactor was observed, which demonstrates that the [Fe](CN)$_2$CO moiety was specifically transferred into the catalytic subunit HyaB.

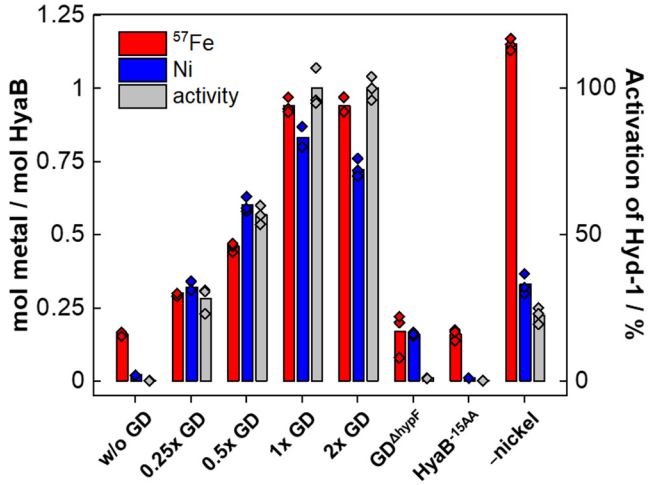

Figure 6. Correlation of the *in vitro* activation of Hyd-1 with the ^{57}Fe and nickel contents of HyaB. Titrating the maturation assay with the ^{57}Fe-labeled GD complex (0.25×–2×) increased the ^{57}Fe and nickel content as well as the Hyd-1 activation. Low levels of 57Fe and nickel and only residual activity were observed when the GD complex lacked the [Fe](CN)$_2$CO moiety (GD$^{\Delta HypF}$) or by employing truncated HyaB^{-15AA}. Excluding nickel from the maturation assay strongly reduced the activation efficiency; however, the ^{57}Fe content of HyaB was barely affected. In contrast, the presence of iron in the active site seems to be prerequisite for nickel insertion. GD, HybG–HypD; Hyd, hydrogenase.

Protein–protein interaction during iron transfer to the active site

To gain additional insights into the specificity of the GD complex to deliver the [Fe]CN$_2$CO moiety for the activation of Hyd-1 and Hyd-2 but not Hyd-3, the binding affinities of the GD complex to the apo-form of the catalytic subunits of Hyd-1 (pre-HyaB), Hyd-2 (pre-HybC), and Hyd-3 (pre-HycE) were determined. For the microscale thermophoresis analysis (MST), the concentration of the dye-labeled catalytic subunits was kept at 50 nM throughout a titration with increasing concentrations of the GD complex. Figure 7*A* depicts how the MST signal for the dye-labeled catalytic subunits pre-HyaB and pre-HybC depends on the GD complex. Fitting these data *via* the Hill equation allowed obtaining the apparent binding affinity (K_d) between the interacting proteins. The data shown in Fig. 7*A* indicate that the GD complex displayed a higher binding affinity to pre-HybC (K_d = 46 ± 4.2 μM) than to pre-HyaB (K_d = 171 ± 24.4 μM). No binding was observed for the interaction between the GD complex and pre-HycE. It was unclear whether the binding of the GD complex to pre-HyaB and pre-HybC is mediated by the GD complex, HybG, or

Table 3
Requirements for Fe transfer into the catalytic subunit during *in vitro* reconstitution of Hyd-1

No.	Reaction mixture	^{57}Fe	^{59}Ni	(% activation)
1	Complete; 2× ^{57}Fe GD [a]	0.94 ± 0.01	0.72 ± 0.03	100
2	Complete; 1× ^{57}Fe GD	0.94 ± 0.02	0.83 ± 0.03	100 ± 6.6
3	Complete; 0.5× ^{57}Fe GD	0.46 ± 0.02	0.60 ± 0.04	57 ± 4.6
4	Complete; 0.25× ^{57}Fe GD	0.30 ± 0.01	0.32 ± 0.03	28 ± 4.5
5	Complete; 1× ^{57}Fe GD$^{\Delta hypF}$ [b]	0.17 ± 0.06	0.16 ± 0.00	0.92 ± 0.03
6	Complete; 1× ^{57}Fe GD^{EDTA} [b]	0.20 ± 0.01	0.01 ± 0.00	0.88 ± 0.03
7	Complete; ^{57}Fe G + ^{57}Fe D	0.25 ± 0.01	0.03 ± 0.00	0.74 ± 0.02
8	Complete; 3× ^{57}Fe CD	0.38 ± 0.01	0.12 ± 0.01	0.17 ± 0.01
9	Complete; aerobic [c]	0.24 ± 0.03	0.19 ± 0.04	8.4 ± 1.7
10	Complete; HyaB^{-15AA}	0.16 ± 0.01	0.01 ± 0.00	0.11 ± 0.04
11	Minus GD complex	0.16 ± 0.01	0.02 ± 0.00	0.13 ± 0.04
12	Minus AM	0.98 ± 0.03	0.17 ± 0.02	0.88 ± 0.06
13	Minus nickel	1.15 ± 0.016	0.33 ± 0.02	22.4± 2.8
14	Minus EF	0.15 ± 0.05	0.016 ± 0.00	1.02 ± 0.04
15	Minus HyaD	0.54 ± 0.02	0.06 ± 0.002	1.1 ± 0.06

The enzyme activities reported are the standard error for 1 representative experiment. The ^{57}Fe and ^{59}Ni metal content was quantified by ICP–MS. The molar ratio (mol metal/mol protein) is calculated based on the molecular mass of the HyaB subunit (66.5 kDa). Metal contents were measured with 2 independent technical replicates. Data are averages of at least 2 independent determinations and reported as the mean ± SD.
[a] A fully ^{57}Fe-labeled GD complex was employed in the maturation assay.
[b] GD complex with no [Fe](CN)$_2$CO was isolated from a *ΔhypF*-mutant strain or was desalted after treating with 10 mM EDTA prior to incubation in the reaction.
[c] Complete reaction mixture was incubated for 60 min in the presence of air prior to activity measurement.

HypD protein. Figure 7*B* reveals that HybG interacts equally well with pre-HyaB (30 ± 29 μM) and pre-HybC (23 ± 2.9 μM), whereas no interaction between HypD and pre-HyaB or pre-HybC was detected. Figure 7*C* shows that the CD complex displayed a higher binding affinity to pre-HycE (K_d = 34 ± 3.2 μM) than to pre-HyaB (K_d = 185 ± 25.1 μM). No detectable binding affinity could be measured for the interaction between the CD complex and pre-HybC. Furthermore, MST experiments suggest a very weak interaction between the GD complex and HyaB^{-15AA}. In summary, these data clearly demonstrate that [Fe](CN)$_2$CO moiety is incorporated into the active site of each Hyd by a specific interaction with the corresponding maturation complex (GD or CD).

Discussion

In the present study, we report a biochemical *in vitro* assay for the study of the maturation of the O$_2$-tolerant [NiFe]-Hyd Hyd-1 of *E. coli*. In previous work, we demonstrated the reconstitution of the O$_2$-sensitive [NiFe]-Hyd Hyd-2 of *E. coli* (20). Both approaches exclusively rely on purified and defined components and thus provide the possibility to elucidate the biogenesis of the [NiFe]-cofactor at the molecular level. The properties of the *in vitro* matured Hyd-1 were comparable to the *in vivo* matured enzyme, for example, the specific H$_2$ uptake activities (27), as well as the FTIR signature under N$_2$, H$_2$, O$_2$, or CO (29–31).

Although major advances in our understanding of the biosynthesis of the [NiFe]-cofactor have been achieved by the group of August Böck (11), we only know certain details about this complex maturation pathway. There is a considerable amount that remains to be understood, for example, neither the metabolic route of CO on the maturation pathway is known nor is anything known about the source of iron in the active site. The map of interactions among the maturation proteins and the sequence of events that occur along the pathway of [NiFe](CN)$_2$CO biosynthesis are not completely understood. Therefore, the development of an *in vitro* reconstitution system was necessary to close the gaps in our understanding of [NiFe]-Hyd maturation. One of the greatest challenges investigating [NiFe]-Hyd maturation *in vivo* is that

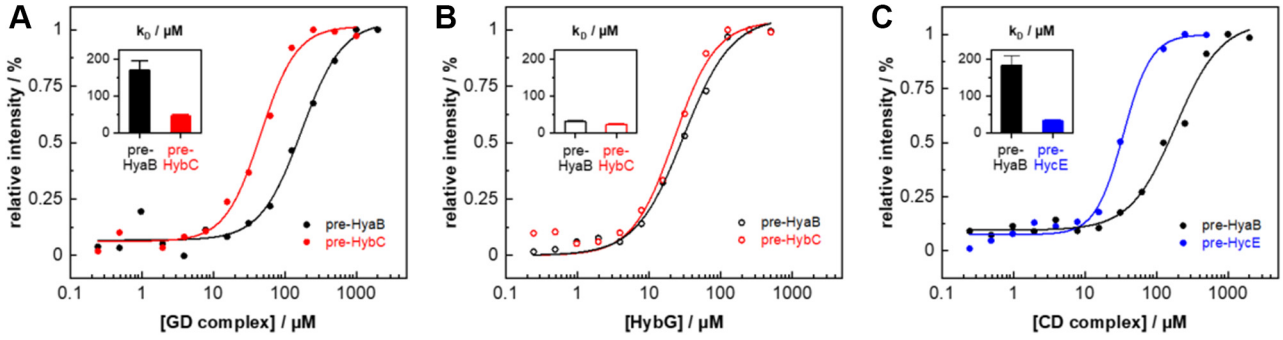

Figure 7. The binding affinities of the catalytic subunit precursors pre-HyaB, pre-HybC, and pre-HycE to GD and HypCD complexes. *A*, GD complex dependence of the MST signal for the fluorescence-labeled pre-HyaB and pre-HybC. *B*, HybG-dependent fluorescence signal of pre-HyaB and pre-HybC. *C*, HypCD complex-dependent fluorescence signal of pre-HycE and pre-HyaB. The MST signals of at least 15 different concentrations of pre-HyaB, pre-HybC, or pre-HycE ranging from 0.1 to 1000 μM were fitted according to Michaelis–Menten kinetics. The *insets* in *panel* depict the obtained binding affinities, K_d. Data of at least 2 independent measurements (n) were combined to create 1 dataset for which the averaged data points as the mean ± SD were fitted by NanoTemper analysis software using a K_d model. The data show higher binding affinities of pre-HyaB and pre-HybC to GD complex and HybG, whereas pre-HycE shows the highest binding affinity to HypCD. The Hill coefficients derived from the fits (Table S1) indicate positive cooperativity (n > 1) in all MST experiments. CD, HypC–HypD; GD, HybG–HypD; MST, microscale thermophoresis analysis.

it cannot necessarily distinguish between the phenotypes of mutants that are impaired in the same biochemical function. For example, although *hypD*, *hype*, and *hypF* are 3 distinct maturation genes, a mutation in any one of them gives exactly the same phenotype, that is, an unprocessed catalytic subunit and inactive Hyd (11). The development of a well-defined *in vitro* reconstitution system allowed us to overcome such problems and exert much greater control over the [NiFe]-Hyd maturation machinery.

In the present study, our *in vitro* reconstitution system was employed to monitor the iron transfer during the maturation process. We could demonstrate direct transfer of ^{57}Fe from ^{57}Fe-labeled GD complex to the catalytic subunit of Hyd-1 (pre-HyaB). Several control experiments suggested that the [Fe](CN)$_2$CO moiety was specifically incorporated into the active site of Hyd-1. Transfer of ^{57}Fe from the GD complex to the active site was observed exclusively when all components of the *in vitro* maturation assay were present; and only very low levels of ^{57}Fe content were found in HyaB when [NiFe]-cofactor assembly was prevented. Our findings are compatible with the assumption that a direct transfer of the [Fe](CN)$_2$CO moiety from the GD complex to pre-HyaB takes place *via* a thiol-disulfide substitution and redox reactions. It has been suggested that the formation of disulfide by oxidation of the cysteines that usually coordinate the active-site cofactor prevents the incorporation of the [Fe](CN)$_2$CO moiety into the active site (11). It is currently unclear why only low levels of ^{57}Fe were transferred from the GD complex to HyaB when HypEF were excluded from the reaction mix, since both accessory proteins are required in early maturation steps for the synthesis and transfer of the CN^- ligands to the GD complex (16, 18). Our data now indicate that their presence is also important for incorporation of the [Fe](CN)$_2$CO into HyaB. We propose that the HypEF complex may facilitate substrate channeling, as suggested earlier (18, 22). It is also conceivable that HypE facilitates dissociation of the GD complex from HyaB upon delivering the [Fe](CN)$_2$CO moiety in order to enter a new cycle of biosynthesis.

The accessory proteins HypA, HypB, and SlyD are specifically involved in the acquisition and insertion of nickel into the catalytic subunit (11, 32). The requirement for these metallochaperones was obviated by the addition of a comparatively high concentration of $NiCl_2$ to the *in vitro* assay (20, 22). Omission of the AM or nickel ions from the maturation assay strongly affected the activation of Hyd-1; however, the ^{57}Fe content of HyaB was not affected at all. These findings indicate that iron incorporation does not rely on the presence of nickel in the active site. In contrast, it can be concluded from all reactions in Table 3 that the insertion of nickel occurs after the insertion of the [Fe](CN)$_2$CO moiety. Our conclusion is supported by isolation of a Hyd large subunit from *Cupriavidus necator* (formerly *Ralstonia eutropha*) that was loaded with the [Fe](CN)$_2$CO moiety but not nickel (33, 34). A similar sequence of events in which iron is delivered first was derived from the observation that nickel is not inserted if the iron maturation proteins are deficient (11, 35, 36).

Although the use of the *in vitro* system has yielded significant information concerning the requirements of iron delivery to the active site of [NiFe]-Hyd, the metabolic source of iron as it enters the maturation was not addressed in the current study. The HybG protein (or its homolog HypC) might be involved in recruiting both the iron and CO_2 molecules for further reductive synthesis of the CO ligand by HypD (13, 14). In future work, we will investigate whether the iron-bound CO_2 ligand coordinated by HybG or HypC has only catalytic function or it ends up in the catalytic site.

It is conceivable that the incorporation of the [Fe](CN)$_2$CO moiety into the active site is based on specific molecular interactions between the GD complex and the catalytic subunit precursor. So far, the exact nature of this interactions and specificity of GD complex to deliver the [Fe](CN)$_2$CO moiety to the catalytic subunit of Hyd-1 and Hyd-2 but not Hyd-3 is poorly understood (23). In this study, MST was applied to determine the binding affinities of the GD and CD complex to the catalytic subunit of the 3 Hyds from *E. coli*. The data show that HybG and not HypD interacts specifically with the large subunit precursor of Hyd-1 and Hyd-2 (pre-HybC and pre-HyaB), whereas its homolog HypC interacts with pre-HycE and has a weaker affinity to pre-HyaB. These findings suggest that the interaction surface of pre-HybC and pre-HyaB to HybG has different structural features than pre-HycE. On the other hand, both HybG and HypC form individually a tight complex with HypD suggesting that HybG and HypC have similar structural features at the interaction surface to HypD. The obtained results support a model in which HypD is a central component during [Fe](CN)$_2$CO synthesis (37), whereas HybG (or its homolog HypC) but not HypD binds specifically to the large subunit precursor of the corresponding Hyd. Overall, the relative affinities of these complexes are on the order of [GD × pre-HybC] > [GD × pre-HyaB], whereas [CD × pre-HycE] > [CD × pre-HyaB] (see Fig. 2 for comparison). It is not completely clear why and how the GD complex specifically binds and mature Hyd-1 and Hyd-2 only while the CD complex is required for the maturation of Hyd-3. Structural comparisons of these precursors will be essential to validate and complement the present results. We suggest that the specificity of the GD and CD complex may determine which [NiFe]-Hyd is matured, depending on the physiological conditions that may require a H_2-evolving enzyme (Hyd-3) or H_2-oxidizing enzymes (Hyd-1 and Hyd-2) (5, 38).

Further downstream along the maturation pathway, our data indicate that the C-terminal extension of HyaB is required for an efficient incorporation of [Fe](CN)$_2$CO into pre-HyaB, as a truncated variant without the C-terminal excision (HyaB^{-15AA}) was devoid of ^{57}Fe. This agrees with our MST data that revealed negligible interaction of the GD complex with the truncated variant HyaB^{-15AA}. These findings are in line with previous pull-down interaction experiments (20) and other studies showing that HybG forms a complex with pre-HybC but not with the truncated variant HybC^{-15AA} (23, 39). We presume that different conformations of the large subunit upon removal of the C-terminal extension may prevent the interaction with the GD complex and thus the iron transfer

(20). Most likely, the C-terminal extension is maintaining in a "correct" conformation to facilitate interaction with the GD complex and to ensure that the active-site cavity remains open until the cofactor is inserted (40, 41).

Taken together, our data demonstrate how the [Fe](CN)$_2$CO cofactor precursor of the GD complex is specifically incorporated into the active site of the corresponding [NiFe]-Hyd. We identified the requirements for the iron incorporation into catalytic subunit during enzyme maturation and provide unprecedented direct evidence for the transfer of iron to the catalytic subunit using ^{57}Fe isotope editing.

Experimental procedures

Bacterial strains and plasmids

All strains and plasmids used are listed in Table 4. To produce the recombinant GD complex, the plasmid pThyp-DEFC^{StrepXT} (14) was digested with NdeI and BamH1 releasing the hypC gene. The PCR-amplified hybG gene was then ligated into the NdeI and BamH1 restriction sites of pT-hypDEF to generate the pT-hypDEFG^{StrepXT} plasmid encoding a twin-Strep-tag fused to HybG at the C terminus. The plasmid pT-hypDEFG^{His} was used to produce the GD complex with a His-tag attached to HybG.

Culture conditions

E. coli strain BL21(DE3) (42) or strains transformed with the indicated plasmids (16, 43) (Table 4) were used as host for overproduction of recombinant proteins. Cultivation of cells was performed in LB medium at 37 °C. Gene expression was induced by the addition of 0.2 μg/ml anhydrotetracycline or 50 μM IPTG followed by continuing incubation at 25 °C for a further 6 h. Cells were harvested when cultures had reached an absorbance of 0.9 to 1.3 by centrifugation at 10,000*g* for 30 min. Washed cell pellets were either used immediately or stored at −80 °C. To produce the ^{57}Fe-labeled GD complex, ^{57}Fe-HypD, and ^{57}Fe-HybG, the bacteria were grown anaerobically in modified M9 minimal medium exactly as described previously (14).

Protein purification

All steps for protein purification were carried out in an anaerobic chamber (Coy Laboratories) under a N_2/H_2 mixture (99:1) and at 4 °C. Wet cell paste containing strep-tagged protein was suspended at a ratio of 1:4 (w/v) in buffer W (100 mM Tris–HCl [pH 8], 150 mM NaCl, 10 mM magnesium acetate, and 1% glycerol) including 2 mM sodium dithionite, 5 μg/ml DNase, and one tablet per 100 ml of Protease Inhibitor Cocktail (Roche). Cells were disrupted by sonication (50 W for 30 min with 0.5 s pulses). Large material and cell debris were removed by centrifugation of the suspension at 15,000*g* for 30 min. The cell-free extract obtained after centrifugation was used directly for anaerobic protein purification by chromatography on a Strep-Tactin-XT column (IBA Lifesciences), exactly as described (14, 20). Wet cell paste containing His-tagged protein was resuspended at a ratio of 1:6 (w/v) in buffer A (50 mM Tris–HCl [pH 8.0] and 300 mM NaCl) including 5 μg/ml DNase and Protease Inhibitor Cocktail. Target protein was isolated by affinity chromatography using cobalt-charged Talon resins (Clontech). Removal of nonspecifically binding contaminants was achieved by washing with 10 column volumes of buffer A, followed by five column volumes of buffer A supplemented with 10 mM imidazole and then three column volumes of buffer A supplemented with 20 to 30 mM imidazole. His-tagged protein was subsequently eluted with buffer A containing 300 mM imidazole. Imidazole was removed by a desalting column and applied to a Superdex 200 gel filtration column. Proteins were concentrated as described previously. For long-term storage, purified protein drops were directly frozen in liquid nitrogen.

The in vitro *reconstitution system of Hyd-1 of* E. coli

The *in vitro* maturation reactions were carried out in an anaerobic chamber (Coy Laboratories) under a N_2/H_2 mixture (99:1). The reaction mixture was prepared in 50 mM Mops KOH (pH 7.0) by combining 4 μM of purified ^{Strep}HyaB and 4 μM of ^{His}GD complex in equimolar amounts; and 2 μM of ^{His}HypE and 2 μM of ^{His}HypF in stoichiometric amounts (20)

Table 4
Strains and plasmids used in this study

Strains/plasmids	Genotype	References
MC4100	F$^-$ *araD139 α(argF-lac)U169 ptsF25 deoC1 relA1 flbB5301 rspL150*$^-$	(52)
BL21(DE3)	F-ompT hsdSB(rB-,mB-)gal dcm (DE3)	Novagen
DHPF-2	MC4100 *ΔhypF*	(16)
FTD147	MC4100 *ΔhyaB ΔhybC ΔhycE*	(43)
Plasmids		
pT-hypCDEF	pT7-7,hypD, HypE, hypC-strep, hypF, Amp^R	(17)
pT-hypDEFG^{StrepXT}	pT7-7, hypD, hypE, hybG-XT-Strep-tag, hypF, Amp^R	This study
pT-hypDEFG^{His}	pT7-7, hypD, hypE, hybG-His-tag, hypF, km^R	This study
pT-hypDEG^{His}	pET30, hypD, hypE, hybG-His-tag, Amp^R	This study
p-hypF	pET28 A, encodes His-HypF, kan^R	(53)
p-hypE	pET28 A, encodes His-HypE, kan^R	(53)
p-hypD	pET28 A, encodes His-HypD, kan^R	(53)
phybGHis	pET30, hybG-His, Amp^R	This study
PC-HyaD	pCA24 N, hyaD, encodes His-HyaD	
pC-hyaB	pET28 A, hybB, encodes His-HyaB, kan^R	This study
pASK-HyaB	pASK-IBA5, hyaB, encodes Strep-HyaB, Amp^R	(53)
pASK-HyaB^{-15AA}	Like pASK-HyaB but without the 15AA C-terminal peptide	This study
pASK-HybC	pASK-IBA5, encodes Strep-HybC, Amp^R	(21)
pASK-HycE	pASK-IBA5, encodes Strep-HycE, Amp^R	(21)
phyaAHis	pET30, hyaA-His, Amp^R	This study

and an AM consisting of 2.5 mM ATP, 50 μM CP, 100 μM $NiCl_2$, and 2 mM sodium dithionite. The reaction mixtures were incubated at RT for 10 to 15 min. The reaction was initiated by the addition of 1 μM of the endopeptidase ^{His}HyaD in catalytic amounts. After incubation on a shaker at ambient temperature (24–26 °C) for further 30 min, 20 μl aliquots of reaction mixture were analyzed by SDS-PAGE. ^{Strep}HyaB was isolated from the reaction mix by Strep-Tactin affinity chromatography applying buffer W containing 300 mM NaCl and 5 mM dithiothreitol, and aliquots of the sample were analyzed for cleavage of HyaB by SDS-PAGE. In the following, the unprocessed large subunit is referred to as pre-HyaB. After puffer exchange, ^{Strep}HyaB preparations were concentrated for infrared spectroscopy and metal analysis. The *in vitro* matured ^{Strep}HyaB protein was mixed with the small subunit of Hyd-1 (^{His}HyaA). Active ^{Strep}HyaB–^{His}HyaA heterodimer was isolated by immobilized metal affinity chromatography *via* cobalt sepharose resin. The activity of Hyd-1 was determined by following the reduction of BV and infrared spectroscopy as reported earlier (44). Large-scale preparation of maturation reaction mix up to 15 ml was applied to isolate preparative amounts of *in vitro* matured ^{Strep}HyaB. In control experiments, various components of the complete reaction mixture were excluded as indicated in the *Results* and *Discussion* sections.

Determination of Hyd activity

Hyd activity was assayed by following the H_2-dependent reduction of BV at 578 nm using an Uvikon 900 dual wavelength spectrophotometer. The activities were measured under strictly anoxic conditions in 1.5 ml anaerobic cuvettes contained 0.8 ml volumes of 4 mM BV in 50 mM Mops buffer at pH 7.0. Cuvettes sealed with rubber stoppers were flushed with a 100% H_2. One unit of H_2 oxidation activity corresponds to the reduction of 2 μmol of BV per min.

PAGE and metal quantification

Protein samples (5–15 μg) were separated by SDS-PAGE (NuPAGE 4–20% Tris–glycine; Invitrogen). Protein MS was applied to confirm the protein identity as described previously (45). Nondenaturing PAGE was applied to analyze the activity of *in vitro* matured Hyd-1 using in-gel activity staining. Protein samples and gel electrophoresis running buffer were supplemented with 4 mM *n*-dodecyl-ß-maltoside. The gel was subsequently stained for enzyme activity as reported previously (10). Protein concentration was determined frequently using the Folin phenol reagent by the procedure originally described by Lowry (46). Protein samples were analyzed for iron, nickel, zinc, and copper by ICP–QqQ–MS as described previously (47).

Infrared spectroscopy

ATR FTIR spectroscopy was carried out in an anaerobic glovebox under a N_2/H_2 mixture (99:1). All spectroscopic experiments were recorded at ambient temperature (24–26 °C) on a Tensor27 FTIR spectrometer (Bruker Optik) as described previously (20, 28, 48). The protein sample (1 μl) was deposited on the three-reflection silicon crystal of an ATR cell, dried under 100% N_2 gas, and rehydrated with buffer solution in the humidified gas stream (28). Reactive gases (H_2, CO, and O_2) were added *via* digital mass flow controllers (Sierra).

Protein interaction studies using MST

Protein-binding experiments were carried out with the Monolith NT.115 (NanoTemper Technologies). Protein labeling was carried out according to the user manuals of the respective labeling kit (RED-NHS or with the dye NT-647). The labeling reaction was carried out for 60 min in the dark at ambient temperature (24–26 °C). Excess dye was removed by a desalting column included in the labeling kit. The buffer used for both protein labeling and MST measurements contained 100 mM Tris–HCl (pH 8), 150 mM NaCl, 10 mM $MgCl_2$, 1% glycerol, and 0.05% Tween-20. Labeled proteins (pre-HyaB, HyaB^{-15AA}, pre-HybC, or pre-HycE) were adjusted to 40 to 50 nM with the buffer mentioned previously. Then, a 16 step 1:1 serial dilution of the "ligand" (GD complex, HybG, HypD, or CD complex) with a final volume of 10 μl was prepared resulting in concentrations from 0.1 to 1000 μM. Next, 10 μl of each dilution was mixed with 10 μl of labeled protein. The mixture was incubated for 30 min and followed by centrifugation at 20,000*g* for 10 min. Afterward, the samples were loaded onto premium MST capillaries. Experiments were carried out at LED settings of 50% power and 50 to 80% MST-laser power.

Quality assessment of purified protein samples

The quality control of purified proteins is the final checkpoint with respect to purity, activity, and integrity. While the H_2 oxidation activity of Hyd-1 is easily monitored (see aforementioned), no Hyd activity is associated with any of the purified (dye labeled) maturation proteins or intermediates used in this study (HyaB, HyaA, HyaD, GD complex, HypE, and HypF). Their catalytic competence was therefore confirmed by the maturation assay established in this study. Furthermore, ATR FTIR was routinely applied to assess the integrity of the $[Fe](CN)_2CO$ cofactor precursor.

Data availability

Strains, mutants, and plasmids that arose from this work will be available on request. All the primary data that are presented in this study can be requested in electronic form by contacting Basem Soboh (basem.soboh@fu-berlin.de).

Supporting information—This article contains supporting information (20, 31).

Acknowledgments—Protein mass spectrometry was done at the Centre for Chemical Microscopy (ProVIS) at UFZ Leipzig.

Author contributions—B. S. conceptualization; B. S., L. A., and S. T. S. methodology; B. S. and S. T. S. software; B. S. and S. T. S. validation; B. S., L. A., and S. T. S. formal analysis; B. S. and S. T. S.

investigation; B. S. and S. T. S. resources; B. S. and S. T. S. data curation; B. S. writing–original draft; B. S. and S. T. S. writing–review & editing; B. S. and S. T. S. visualization; B. S. supervision; B. S. project administration; B. S. and S. T. S. funding acquisition.

Funding and additional information—This work was supported by German Research Foundation *via* the SPP 1927 priority program "Iron-Sulfur for Life," grant nos.: SO1325/5-2 (to B. S.) and STR1554/5-1 (to S. T. S.).

Conflict of interest—The authors declare that they have no conflicts of interest with the contents of this article.

Abbreviations—The abbreviations used are: AM, activation mix; ATR, attenuated total reflection; BV, benzyl viologen; CD, HypC–HypD; GD, HybG–HypD; Hyd, hydrogenase; ICP, inductively coupled plasma; MS, mass spectrometry; MST, microscale thermophoresis analysis.

References

1. Vignais, P. M., and Billoud, B. (2007) Occurrence, classification, and biological function of hydrogenases: an overview. *Chem. Rev.* **107**, 4206–4272
2. Thauer, R. K., Kaster, A. K., Goenrich, M., Schick, M., Hiromoto, T., and Shima, S. (2010) Hydrogenases from methanogenic archaea, nickel, a novel cofactor, and H-2 storage. *Annu. Rev. Biochem.* **79**, 507–536
3. Lubitz, W., Ogata, H., Rudiger, O., and Reijerse, E. (2014) Hydrogenases. *Chem. Rev.* **114**, 4081–4148
4. Shafaat, H. S., Rudiger, O., Ogata, H., and Lubitz, W. (2013) [NiFe] hydrogenases: a common active site for hydrogen metabolism under diverse conditions. *Biochim. Biophys. Acta* **1827**, 986–1002
5. Sargent, F. (2016) The model [NiFe]-Hydrogenases of Escherichia coli. *Adv. Microb. Physiol.* **68**, 433–507
6. Forzi, L., and Sawers, R. G. (2007) Maturation of [NiFe]-hydrogenases in Escherichia coli. *Biometals* **20**, 565–578
7. Lukey, M. J., Roessler, M. M., Parkin, A., Evans, R. M., Davies, R. A., Lenz, O., *et al.* (2011) Oxygen-tolerant [NiFe]-hydrogenases: the individual and collective importance of supernumerary cysteines at the proximal Fe-S cluster. *J. Am. Chem. Soc.* **133**, 16881–16892
8. Sawers, R. G., Ballantine, S. P., and Boxer, D. H. (1985) Differential expression of hydrogenase isoenzymes in Escherichia coli K-12: evidence for a third isoenzyme. *J. Bacteriol.* **164**, 1324–1331
9. Laurinavichene, T. V., and Tsygankov, A. A. (2001) H2 consumption by Escherichia coli coupled via hydrogenase 1 or hydrogenase 2 to different terminal electron acceptors. *FEMS Microbiol. Lett.* **202**, 121–124
10. Ballantine, S. P., and Boxer, D. H. (1985) Nickel-containing hydrogenase isoenzymes from anaerobically grown Escherichia coli K-12. *J. Bacteriol.* **163**, 454–459
11. Böck, A., King, P. W., Blokesch, M., and Posewitz, M. C. (2006) Maturation of hydrogenases. *Adv. Microb. Physiol.* **51**, 1–71
12. Lacasse, M. J., and Zamble, D. B. (2016) [NiFe]-Hydrogenase maturation. *Biochemistry* **55**, 1689–1701
13. Soboh, B., Stripp, S. T., Bielak, C., Lindenstrauss, U., Braussemann, M., Javaid, M., *et al.* (2013) The [NiFe]-hydrogenase accessory chaperones HypC and HybG of Escherichia coli are iron- and carbon dioxide-binding proteins. *FEBS Lett.* **587**, 2512–2516
14. Stripp, S. T., Oltmanns, J., Muller, C. S., Ehrenberg, D., Schlesinger, R., Heberle, J., *et al.* (2021) Electron inventory of the iron-sulfur scaffold complex HypCD essential in [NiFe]-hydrogenase cofactor assembly. *Biochem. J.* **478**, 3281–3295
15. Nutschan, K., Golbik, R. P., and Sawers, R. G. (2019) The iron-sulfur-containing HypC-HypD scaffold complex of the [NiFe]-hydrogenase maturation machinery is an ATPase. *Febs Open Bio* **9**, 2072–2079
16. Paschos, A., Bauer, A., Zimmermann, A., Zehelein, E., and Böck, A. (2002) HypF, a carbamoyl phosphate-converting enzyme involved in [NiFe] hydrogenase maturation. *J. Biol. Chem.* **277**, 49945–49951
17. Blokesch, M., Albracht, S. P., Matzanke, B. F., Drapal, N. M., Jacobi, A., and Böck, A. (2004) The complex between hydrogenase-maturation proteins HypC and HypD is an intermediate in the supply of cyanide to the active site iron of [NiFe]-hydrogenases. *J. Mol. Biol.* **344**, 155–167
18. Stripp, S. T., Lindenstrauss, U., Sawers, R. G., and Soboh, B. (2015) Identification of an isothiocyanate on the HypEF complex suggests a route for efficient Cyanyl-group channeling during [NiFe]-hydrogenase cofactor generation. *PLoS One* **10**, e0133118
19. Stripp, S. T., Lindenstrauss, U., Granich, C., Sawers, R. G., and Soboh, B. (2014) The influence of oxygen on [NiFe]-hydrogenase cofactor biosynthesis and how ligation of carbon monoxide precedes cyanation. *PLoS One* **9**, e107488
20. Senger, M., Stripp, S. T., and Soboh, B. (2017) Proteolytic cleavage orchestrates cofactor insertion and protein assembly in [NiFe]-hydrogenase biosynthesis. *J. Biol. Chem.* **292**, 11670–11681
21. Pinske, C., Kruger, S., Soboh, B., Ihling, C., Kuhns, M., Braussemann, M., *et al.* (2011) Efficient electron transfer from hydrogen to benzyl viologen by the [NiFe]-hydrogenases of Escherichia coli is dependent on the coexpression of the iron-sulfur cluster-containing small subunit. *Arch. Microbiol.* **193**, 893–903
22. Soboh, B., Lindenstrauss, U., Granich, C., Javed, M., Herzberg, M., Thomas, C., *et al.* (2014) [NiFe]-hydrogenase maturation *in vitro*: analysis of the roles of the HybG and HypD accessory proteins1. *Biochem. J.* **464**, 169–177
23. Blokesch, M., Magalon, A., and Böck, A. (2001) Interplay between the specific chaperone-like proteins HybG and HypC in maturation of hydrogenases 1, 2, and 3 from Escherichia coli. *J. Bacteriol.* **183**, 2817–2822
24. Blokesch, M., and Bock, A. (2006) Properties of the [NiFe]-hydrogenase maturation protein HypD. *Febs Lett.* **580**, 4065–4068
25. Rossmann, R., Maier, T., Lottspeich, F., and Böck, A. (1995) Characterisation of a protease from Escherichia coli involved in hydrogenase maturation. *Eur. J. Biochem.* **227**, 545–550
26. Theodoratou, E., Huber, R., and Böck, A. (2005) [NiFe]-Hydrogenase maturation endopeptidase: structure and function. *Biochem. Soc. Trans.* **33**, 108–111
27. Lukey, M. J., Parkin, A., Roessler, M. M., Murphy, B. J., Harmer, J., Palmer, T., *et al.* (2010) How Escherichia coli is equipped to oxidize hydrogen under different redox conditions. *J. Biol. Chem.* **285**, 3928–3938
28. Stripp, S. T. (2021) *In Situ* infrared spectroscopy for the analysis of gas-processing metalloenzymes. *ACS Catal.* **11**, 7845–7862
29. Hidalgo, R., Ash, P. A., Healy, A. J., and Vincent, K. A. (2015) Infrared spectroscopy during electrocatalytic turnover reveals the Ni-L active site state during H2 oxidation by a NiFe hydrogenase. *Angew. Chem. Int. Ed. Engl.* **54**, 7110–7113
30. Murphy, B. J., Hidalgo, R., Roessler, M. M., Evans, R. M., Ash, P. A., Myers, W. K., *et al.* (2015) Discovery of dark pH-dependent H(+) migration in a [NiFe]-hydrogenase and its mechanistic relevance: mobilizing the hydrido ligand of the Ni-C intermediate. *J. Am. Chem. Soc.* **137**, 8484–8489
31. Ash, P. A., Hidalgo, R., and Vincent, K. A. (2017) Proton transfer in the catalytic cycle of [NiFe] hydrogenases: insight from vibrational spectroscopy. *ACS Catal.* **7**, 2471–2485
32. Watanabe, S., Kawashima, T., Nishitani, Y., Kanai, T., Wada, T., Inaba, K., *et al.* (2015) Structural basis of a Ni acquisition cycle for [NiFe] hydrogenase by Ni-metallochaperone HypA and its enhancer. *Proc. Natl. Acad. Sci. U.S.A.* **112**, 7701–7706
33. Winter, G., Buhrke, T., Lenz, O., Jones, A. K., Forgber, M., and Friedrich, B. (2005) A model system for [NiFe] hydrogenase maturation studies: purification of an active site-containing hydrogenase large subunit without small. *Febs Lett.* **579**, 4292–4296
34. Loscher, S., Zebger, I., Andersen, L. K., Hildebrandt, P., Meyer-Klaucke, W., and Haumann, M. (2005) The structure of the Ni-Fe site in the isolated HoxC subunit of the hydrogen-sensing hydrogenase from Ralstonia eutropha. *Febs Lett.* **579**, 4287–4291
35. Theodoratou, E., Paschos, A., Magalon, A., Fritsche, E., Huber, R., and Böck, A. (2000) Nickel serves as a substrate recognition motif for the

endopeptidase involved in hydrogenase maturation. *Eur. J. Biochem.* **267**, 1995–1999
36. Blokesch, M., and Bock, A. (2002) Maturation of [NiFe]-hydrogenases in Escherichia coli: the HypC cycle. *J. Mol. Biol.* **324**, 287–296
37. Stripp, S. T., Soboh, B., Lindenstrauss, U., Braussemann, M., Herzberg, M., Nies, D. H., *et al.* (2013) HypD is the scaffold protein for Fe-(CN)2CO cofactor assembly in [NiFe]-hydrogenase maturation. *Biochemistry* **52**, 3289–3296
38. Haase, A., and Sawers, R. G. (2022) Exchange of a single amino acid residue in the HybG chaperone allows maturation of all H2-activating [NiFe]-Hydrogenases in Escherichia coli. *Front Microbiol.* **13**, 872581
39. Thomas, C., Muhr, E., and Sawers, R. G. (2015) Coordination of synthesis and assembly of a modular membrane-associated [NiFe]-hydrogenase is determined by cleavage of the C-terminal peptide. *J. Bacteriol.* **197**, 2989–2998
40. Kwon, S., Watanabe, S., Nishitani, Y., Kawashima, T., Kanai, T., Atomi, H., *et al.* (2018) Crystal structures of a [NiFe] hydrogenase large subunit HyhL in an immature state in complex with a Ni chaperone HypA. *Proc. Natl. Acad. Sci. U.S.A.* **115**, 7045–7050
41. Pinske, C., Thomas, C., Nutschan, K., and Sawers, R. G. (2019) Delimiting the function of the C-terminal extension of the Escherichia coli [NiFe]-hydrogenase 2 large subunit precursor. *Front Microbiol.* **10**, 2223
42. Studier, F. W., and Moffatt, B. A. (1986) Use of bacteriophage T7 RNA polymerase to direct selective high-level expression of cloned genes. *J. Mol. Biol.* **189**, 113–130
43. Redwood, M. D., Mikheenko, I. P., Sargent, F., and Macaskie, L. E. (2008) Dissecting the roles of Escherichia coli hydrogenases in biohydrogen production. *FEMS Microbiol. Lett.* **278**, 48–55
44. Senger, M., Mebs, S., Duan, J., Wittkamp, F., Apfel, U. P., Heberle, J., *et al.* (2016) Stepwise isotope editing of [FeFe]-hydrogenases exposes cofactor dynamics. *Proc. Natl. Acad. Sci. U.S.A.* **113**, 8454–8459
45. Seidel, K., Kuhnert, J., and Adrian, L. (2018) The complexome of Dehalococcoides mccartyi reveals its organohalide respiration-complex is modular. *Front Microbiol.* **9**, 1130
46. Lowry, O. H., Rosebrough, N. J., Farr, A. L., and Randall, R. J. (1951) Protein measurement with the Folin phenol reagent. *J. Biol. Chem.* **193**, 265–275
47. Budhraja, R., Ding, C., Walter, P., Wagner, S., Reemtsma, T., Gary Sawers, R., *et al.* (2019) The impact of species, respiration type, growth phase and genetic inventory on absolute metal content of intact bacterial cells. *Metallomics* **11**, 925–935
48. Senger, M., Laun, K., Soboh, B., and Stripp, S. T. (2018) Infrared Characterization of the bidirectional oxygen-sensitive [NiFe]-hydrogenase from E-coli. *Catalysts* **8**
49. Menon, N. K., Chatelus, C. Y., Dervartanian, M., Wendt, J. C., Shanmugam, K. T., Peck, H. D., Jr., *et al.* (1994) Cloning, sequencing, and mutational analysis of the Hyb operon encoding Escherichia coli hydrogenase 2. *J. Bacteriol.* **176**, 4416–4423
50. Soboh, B., Stripp, S. T., Muhr, E., Granich, C., Braussemann, M., Herzberg, M., *et al.* (2012) [NiFe]-hydrogenase maturation: Isolation of a HypC-HypD complex carrying diatomic CO and CN- ligands. *FEBS Lett.* **586**, 3882–3887
51. Shomura, Y., and Higuchi, Y. (2012) Structural basis for the reaction mechanism of S-carbamoylation of HypE by HypF in the maturation of [NiFe]-hydrogenases. *J. Biol. Chem.* **287**, 28409–28419
52. Casadaban, M. J. (1976) Transposition and fusion of lac genes to selected promoters in Escherichia-coli using bacteriophage-lambda and bacteriophage-Mu. *J. Mol. Biol.* **104**, 541–555
53. Soboh, B., Kruger, S., Kuhns, M., Pinske, C., Lehmann, A., and Sawers, R. G. (2010) Development of a cell-free system reveals an oxygen-labile step in the maturation of [NiFe]-hydrogenase 2 of Escherichia coli. *FEBS Lett.* **584**, 4109–4114